Nanoscale

RSC Publishing

PAPER

View Article Online
View Journal | View Issue

Microstructural evolution of carbon nanotube fibers: deformation and strength mechanism†

Cite this: *Nanoscale*, 2013, **5**, 2002

Xia Liu,[ab] Weibang Lu,*[bc] Orlando M. Ayala,[b] Lian-Ping Wang,[b] Anette M. Karlsson,[b] Qingsheng Yang[a] and Tsu-Wei Chou*[bc]

A comprehensive investigation of the mechanical behavior and microstructural evolution of carbon nanotube (CNT) continuous fibers under twisting and tension is conducted using coarse-grained molecular dynamics simulations. The tensile strength of CNT fibers with random CNT stacking is found to be higher than that of fibers with regular CNT stacking. The factor dominating the mechanical response of CNT fibers is identified as individual CNT stretching. A simplified twisted CNT fiber model is studied to illustrate the structural evolution mechanisms of CNT fibers under tension. Moreover, it is demonstrated that CNT fibers can be reinforced by enhancing intertube interactions. This study would be helpful not only in the general understanding of the nano- and micro-scale factors affecting CNT fibers' mechanical behavior, but also in the optimal design of CNT fibers' architecture and performance.

Received 9th September 2012
Accepted 4th January 2013

DOI: 10.1039/c3nr32681k

www.rsc.org/nanoscale

1 Introduction

Multiscale carbon nanotube (CNT) assemblies, ranging from nanoscopic CNT bundles to microscopic CNT films to macroscopic CNT arrays and fibers, present fascinating basic research opportunities with significant technological implications. The processing of continuous fibers based on CNTs offers a unique demonstration of the evolution of CNT structures at various length scales as well as the opportunity to identify key contributing factors driving the fiber performance.[1,2] In 2002, Jiang *et al.*[3] first spun a 30 cm long CNT fiber from a free-standing vertically aligned CNT array. Since then, significant efforts have been made by researchers worldwide in processing continuous films and fibers based on CNT arrays (or forests).[1] The processability of continuous fibers was attributed to the high quality and regular structure of the super-aligned CNT array.[4] So far, experiments have indicated that the tensile strength of CNT fibers spun from CNT forests varies from hundreds of MPa to about 3 GPa.[5–12]

Since the dry-spinning of CNT fibers involves drawing of a film-like precursor from a vertically aligned CNT array, it is essential to gain a basic understanding of the mechanism of film formation and its correlation with resulting film properties. Here, we consider two important experimental observations during CNT film formation and drawing processes. One is that CNTs in the highly aligned arrays always form tight bundles, which indicates strong van der Waals (vdW) interactions among CNTs.[8–11,13] Another is that CNT bundles are peeled off from an array in a consistent manner, namely, from the top to the bottom of the array, and then from the bottom back up to the top.[4,14] In this manner, CNTs are transformed from a vertically aligned array into a continuous film in which neighbouring layers of CNTs form end-to-end junctions.[4] Using an optical microscope, Liu *et al.*[14] validated the presence of these end-to-end junctions from *in situ* recording of the CNT film forming process. These CNT junctions might play a pivotal role in the formation of films and influence their morphological and mechanical properties.

Besides the structural evolution during the process of drawing a CNT film from an array, further reorganization of the CNTs takes place during the subsequent twisting and stretching processes. For example, the twisting of a CNT film to a fiber induces radial compressive stress among the CNTs, which densifies the CNT fiber and enhances the load transfer efficiency between neighbouring CNTs in the fiber, thus giving rise to enhancements in CNT fiber strength. A surface twist angle, which is defined as the angle between the axis of CNTs on the fiber surface and the fiber axis, has been used to represent the extent of twist of a CNT fiber.[4,8,10,12,15–19] The work of Zhang *et al.*[10] demonstrated that increasing the twist angle from 10° to 21° gave rise to an increase in CNT fiber tensile strength from 0.17 GPa to 0.41 GPa. Aside from this positive effect of twisting, the twisting induced obliquity of CNTs in the fiber could negatively impact the fiber mechanical properties. Researchers have found that, after exceeding an optimal twisting angle, additional twisting would result in a decrease in fiber modulus and strength.[16,17]

[a]*Department of Engineering Mechanics, Beijing University of Technology, Beijing 100124, PR China*

[b]*Department of Mechanical Engineering, University of Delaware, Newark, Delaware 19716, USA. E-mail: weibang@udel.edu*

[c]*Center for Composite Materials, University of Delaware, Newark, Delaware 19716, USA. E-mail: chou@udel.edu; Fax: +1 302-831-3619; Tel: +1 302-831-1550*

† Electronic supplementary information (ESI) available. See DOI: 10.1039/c3nr32681k

While extensive efforts have been made in the areas of CNT fiber fabrications and experimental characterizations of their physical and mechanical properties,[1] there remains a lack of detailed analysis of their microstructural evolution. The goal of the present work is to provide a comprehensive investigation of the fiber microstructural evolution during the fiber forming and stretching processes based on the coarse-grained (CG) molecular dynamics (MD) simulations. Besides, the effects of some key factors, such as CNT distribution, fiber twisting as well as intertube interactions, on the mechanical performance of CNT fibers have also been investigated.

2 CGMD simulation method

Since a CNT-based fiber is composed of a large number of CNTs, and there exist complex pairwise inter-tube van der Waals (vdW) interactions, it is therefore computationally prohibitive to simulate the fiber structural evolution using full atomistic MD simulations. Here, we adopt a CGMD simulation technique[20] to establish a mesoscale model of the CNTs; this approach has been successfully implemented to explore the structural evolution and mechanical properties of large-area CNT arrays,[21] CNT networks[22,23] as well as buckypapers.[24–26]

In CGMD simulations, a single CNT is represented by a bead–spring model consisting of a series of beads connected by springs, as shown in Fig. 1. Due to the fact that CNTs in the film/fiber are discontinuous, the torsional freedom of individual CNTs is only slightly restricted during the fiber twisting. Meanwhile, CNTs in the fiber are of high aspect ratio. So intertube vdW interactions play a dominant role in the film twisting (see ESI for the discussion of CNT torsion†). Thus, deformation of the CNTs is described by the elongation of the springs due to stretching and the change of angles between two neighbouring springs in the CNTs due to bending, while CNT torsion is not considered in the current study. The energies related to stretching and bending of springs can be expressed as

$$E_{\mathrm{T}} = \frac{1}{2}k_{\mathrm{T}}(r - r_0)^2 \tag{1}$$

and

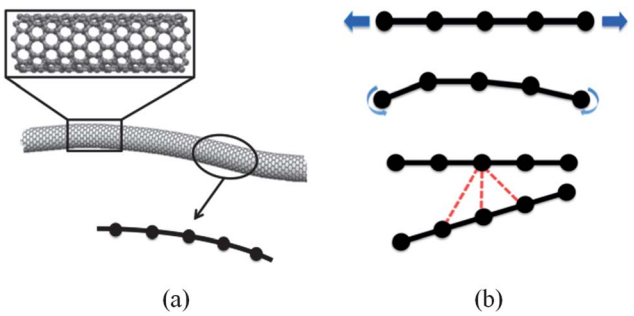

Fig. 1 Schematic illustration of the CG model for a CNT. (a) The fully atomistic CNT model is replaced by a line of beads connected *via* springs. (b) Elongation of the springs in the CNT due to stretching (top), change of angles between two neighbouring springs in the CNT due to bending (middle) and adjacent CNTs interact with each other *via* vdW forces between the beads (bottom).

Table 1 Summary of mesoscopic parameters used for CNTs (5,5)

Parameters	Values	Units
Equilibrium distance, r_0	50	Å
Tensile stiffness, k_{T}	200	kcal mol^{-1} Å^{-2}
Equilibrium angle, θ_0	180	degree
Bending stiffness, k_θ	2875.4	kcal mol^{-1} rad^{-2}
Dispersive parameter, ε	83.236	Å
Dispersive parameter, σ	24.157	kcal mol^{-1}

$$E_\theta = \frac{1}{2}k_\theta(\theta - \theta_0)^2 \tag{2}$$

where k_{T} and k_θ denote bond stiffness and angle stiffness, while r_0 and θ_0 represent the equilibrium spring length and angle between neighboring springs. The adjacent CNTs interact with each other *via* vdW forces between the beads and the interbeads energy can be computed as

$$E_{\mathrm{pair}} = 4\varepsilon\left[\left(\frac{\sigma}{d}\right)^{12} - \left(\frac{\sigma}{d}\right)^{6}\right] \tag{3}$$

where σ is the distance parameter, ε is the energy well depth at equilibrium and d is the distance between two interacting beads. Thus, the total potential energy of a CNT assembly can be expressed as

$$\begin{aligned} E_{\mathrm{total}} &= \sum E_{\mathrm{T}} + \sum E_\theta + \sum E_{\mathrm{pair}} \\ &= \sum \frac{1}{2}k_{\mathrm{T}}(r - r_0)^2 + \sum \frac{1}{2}k_\theta(\theta - \theta_0)^2 + \sum 4\varepsilon\left[\left(\frac{\sigma}{d}\right)^{12} - \left(\frac{\sigma}{d}\right)^{6}\right] \end{aligned} \tag{4}$$

All of the parameters can be obtained by a series of full MD atomistic calculations of mechanical tests. Details of the derivation can be found in ref. 20. For the sake of computation efficiency, we focus this study on the behavior of assemblies of CNTs (5,5). The parameters of the CG model of a CNT (5,5) are given in Table 1.

The CG simulations were carried out using Sandia Laboratory's large-scale atomic/molecular massively parallel simulator (LAMMPS) code, which is specifically designed to run on parallel computer systems and has good scaling characteristics on a wide range of high performance computing (HPC) platforms.[27]

3 Results and discussion

3.1 CNT film models

In reality, long continuous CNT films/fibers are composed of short individual CNTs. So in this study, CNT films and fibers are composed of discrete CNTs, instead of continuous ones. Two types of CNT film models have been developed; in one of the model CNTs are randomly stacked, while in the other CNTs are regularly stacked, as shown in Fig. 2a and b, respectively. The details of the models are given as follows. (1) Two layers of CNT films with 2 nm interlayer distance are first constructed. In each layer, there are 19 continuous CNTs, and the distance between neighboring CNTs is 2 nm. The length of each layer is 1 μm.

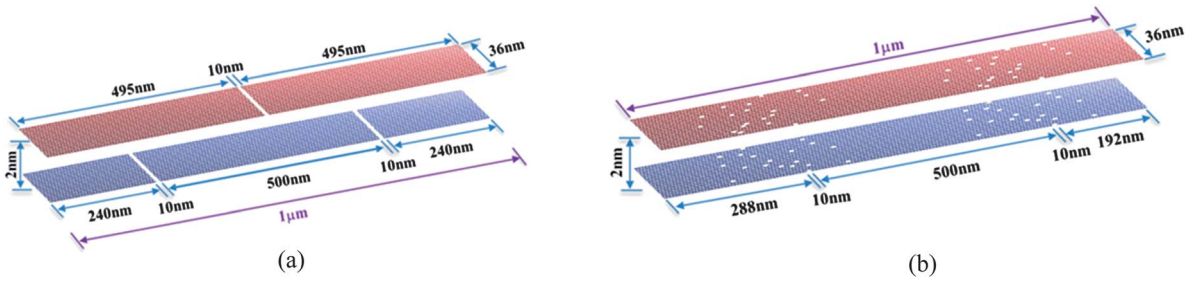

Fig. 2 Initial coarse-grained models of CNT films with (a) regular stacking and (b) random stacking. The red and blue lines represent CNTs on top and bottom layers of the film, respectively. The spacing among CNTs at the same layer as well as the distance between two layers are enlarged for better distinction.

Thus, the size of the CNT film is 1 μm × 36 nm × 2 nm. (2) To construct the regular CNT stacking film model, a strip of central 10 nm long CNTs in the upper layer and two strips of 10 nm long CNTs in the lower layer are discarded, as shown in Fig. 2a. (3) To construct the random CNT stacking film model, two 10 nm long CNT segments in each CNT are discarded at random positions (on the condition that the resulting central segment is 500 nm long), as shown in Fig. 2b. CNTs at the top and bottom layers of the film are coloured in red and blue for better distinction. For the whole CNT film model, the total number of beads is 7581 and 7562 for regular and random CNT stacking films, respectively.

During each simulation, random velocities are first assigned to each bead of the CNT film to attain a desired initial temperature of 300 K. The computation time step is 1 fs in the present study. The CNT film models are then relaxed to reach an equilibrium state over a simulation time of 1 ns, which ensures numerical convergence of integration. A microcanonical NVE ensemble, which describes a system with a fixed number of particles (N), fixed volume (V) and fixed energy (E), is applied for energy conservation of the model. Afterwards, simulations of the twisting process from the equilibrated CNT films to fibers are performed by applying torsion to the film ends in opposite directions with a rate of 360° per 100 000 fs. Afterwards, during the simulation of fiber tension, a uniform axial strain rate of 0.0001 per 500 000 fs is applied to one end of the fiber while keeping another end fixed.

3.2 Reorganization of CNT films under rotation

Twisting simulations are carried out on the above-mentioned equilibrated CNT films. Configurations of CNT fibers twisted from CNT films with random and regular end stacking are described in Fig. 3a and b. In both fibers, CNTs are curled up under the external twist loading and bundled by the inter-tube vdW forces. However, a remarkable difference in crisscross and winding patterns can be found in these two types of fibers. In the fiber obtained from a CNT film with random CNT stacking, CNTs in different layers bundle into a uniform cylinder under the coupling effect of twisting and vdW interactions, as shown in Fig. 3a. However, the fiber obtained from a CNT film with regular CNT stacking displays a significantly different morphology: the CNTs form a distinct, uniform crisscross pattern in some regions; however, this pattern unravels at the overlapped regions of the fiber due to insufficient vdW interactions, as shown in Fig. 3b. Thus, the fiber diameter at these overlapped areas is larger than that at the other area. The morphology also shows that the CNT ends in the fiber with regular stacking are concentrated and form weak cross-sections while the ends in the fiber with random stacking are scattered after twisting.

To gain an insight into the microstructural evolution during the twisting process, the evolution of potential energy, generated from spring stretching, spring angle bending and the vdW interactions between CNTs, is recorded during the twisting process of the regular CNT stacking film. Variations of these energy components with applied rotation are plotted in Fig. 4. The total potential energy is found to increase with twisting. Initially, the CNTs are stretched and bent resulting in an increase in spring stretching and bending energy. Meanwhile, the vdW energy decreased (absolute value increased) due to the twist induced densification of the CNT fiber. Once the fiber is twisted beyond 5 turns, however, the interfacial stress among CNTs reaches its ultimate value that is insufficient to maintain the tensile stress. Consequently, some CNTs slide with respect to each other and the spring stretching energy is released until reaching a steady state. Meanwhile, the intertube vdW energy increased (absolute value decreased) during this period mainly due to intertube sliding.

3.3 Mechanical response of twisted fiber under tension

In a CNT fiber, the inevitable tube ends signify the discontinuities in CNT load-carrying capability when the fiber is under tension. To gain insight into the relationship between microstructural characteristics and macroscopic mechanical behavior, tensile simulations are conducted on both regular and random CNT fibers. Variations of the tensile strength of these two types of CNT fibers (both are 1 μm in length) with increasing twist are illustrated in Fig. 5a. These simulations demonstrate that the highest tensile strength is 0.62 GPa and 0.57 GPa for random and regular CNT stacking fibers, respectively. The difference shown in their tensile response clearly demonstrates the benefits of random CNT stacking along the fiber length. In addition, it is interesting to note that the fiber tensile strength is initially enhanced with increasing twist. The highest fiber strength is reached after 2 full turns of rotation while the strength drops subsequently with further twisting.

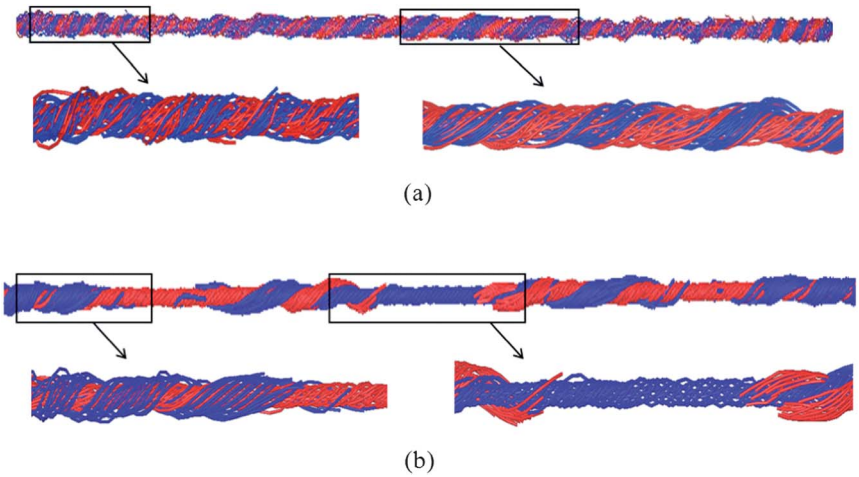

Fig. 3 Structural reorganization of (a) fiber with random CNT stacking and (b) fiber with regular CNT stacking after twisting. Enlarged images show the morphologies at different sections of the fibers. The CNTs in the top and bottom layers of the CNT film are colored in red and blue, respectively.

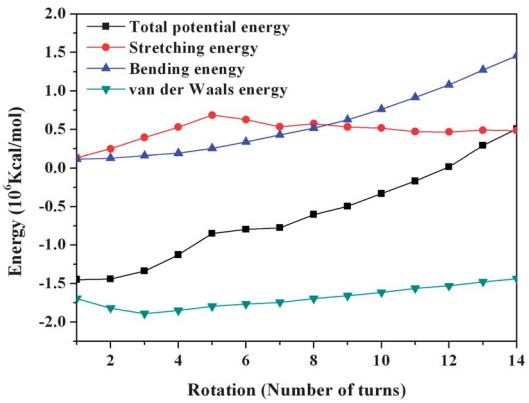

Fig. 4 Variations of potential energy in the CNT fiber with random stacking under rotation.

The effect of twisting on the fiber strength obtained here is consistent with that concluded from experimental characterizations.[16,18] The increase in strength at low rotation angles may be attributed to an enhancement in vdW interactions between CNTs, while the reduction in strength after optimal rotation can be attributed to the large off-axis angle of the CNTs induced by fiber twisting. The trade-off between tightening the nanotubes (higher vdW interaction and better load transfer) and nanotube axial load carrying capability (better alignment) needs to be taken into account in the optimal design of fiber strength. Furthermore, typical tensile stress–strain relationships of the random fiber with small twisting angles are given in Fig. 5b. Each of these curves has two stages. In the first stage, the fiber stress increases nearly linearly with strain because of the CNT stretching; and in the second stage, the fiber stress oscillates due to continuing bond stretching and intertube sliding.

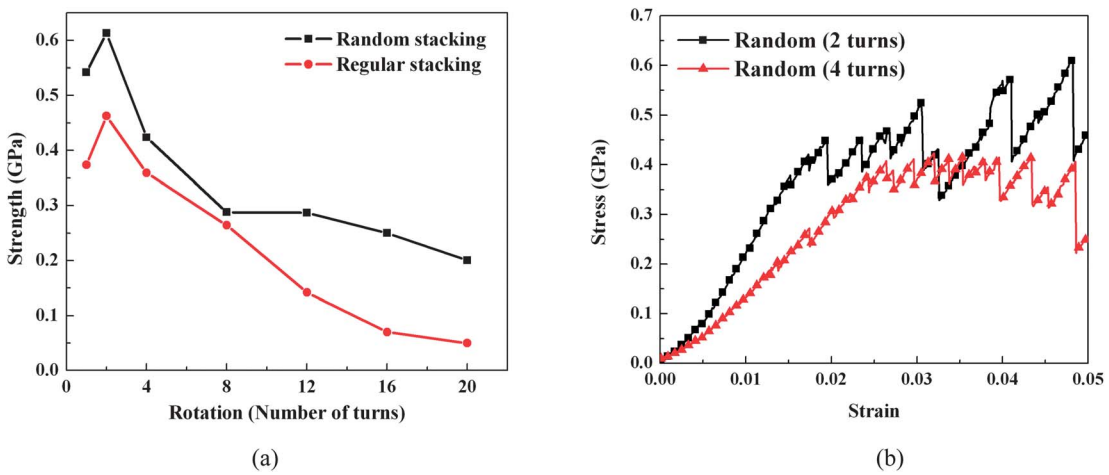

Fig. 5 (a) Comparison of the strength of twisted CNT fibers with random end stacking and regular end stacking under different rotation turns and (b) typical stress–strain curves of CNT fibers with random end stacking.

To further identify the contributions to the axial tensile stress in the CNT fiber, the axial stress is decomposed into three categories, which are attributed to bond stretching, bond angle bending and vdW interactions, according to eqn (4) in the section of the CGMD method. The same decomposition has been employed to identify the relationship between the micro-structural characteristics and macroscopic mechanical behavior of CNT networks.[22] As shown in Fig. 6, the bond stretching term, $\sigma_{z\text{-bond}}$, plays a dominant role, while the bond angle term $\sigma_{z\text{-angle}}$ and the vdW interaction term $\sigma_{z\text{-vdW}}$ are much smaller. This fact has also been noticed during the deformation of films with randomly distributed CNTs.[22] Thus, to obtain a CNT fiber with better mechanical performance, higher individual CNT stretching is needed. In other words, more CNTs along the axial direction are needed to bear tensile loads after the densification *via* twisting. Moreover, by tracking the change in the length of the CNT bonds in the two CNT fibers during the whole tension process, it is revealed that all the tensile strains of CNTs in the fiber are below 2%, which is significantly lower than their failure strain of about 16%.[28] Consequently, if only intertube vdW forces are responsible for the stress transference among the CNTs within the fibers, the superior mechanical properties of the individual CNTs are hardly brought into full play.

It should be mentioned that when the two ends of a twisted CNT fiber are set free before stretching, the fiber will untwist to some extent, but will not return to the untwisted state. The larger the twist angle is, the higher degree of fiber untwist will be. The untwisting of a CNT fiber can be illustrated by the decrease of the total bending energy of the CNTs, as shown in Fig. 7, due to the unbending of individual CNTs. Thus, in the present study, two ends of the fibers are fixed during the whole process of twisting and stretching to avoid the influence of untwisting on the relationship between fiber strength and the level of rotation.

3.4 Structural evolution mechanism of twisted CNT fibers

A simplified coarse-grained CNT fiber model, which consists of seven CNTs in the cross-section, is constructed aiming to clearly illustrate the structural evolution of the twisted fiber under tension. CNTs in this model are randomly distributed. Fig. 8a shows the stress–strain curve of the CNT fiber under tension. The whole deformation process can be divided into two stages. In the first stage range, which is from the initial state to the

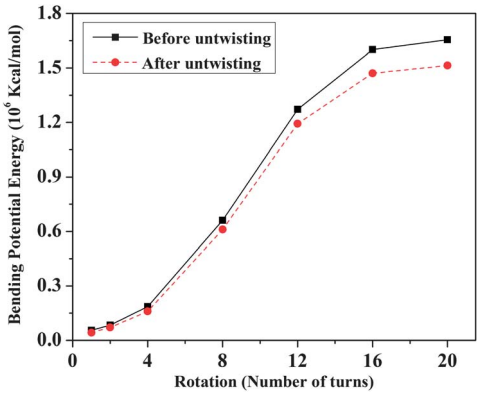

Fig. 7 Variation of bending potential energy before and after untwisting.

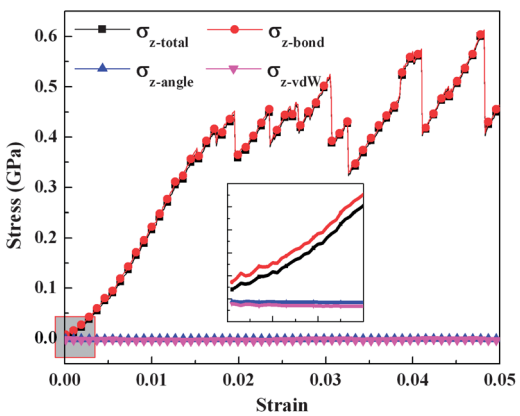

Fig. 6 The relationship between the total fiber tensile stress and strain, with decomposition of $\sigma_{z\text{-total}}$ into contributions from bond stretching, $\sigma_{z\text{-bond}}$, bond angle bending, $\sigma_{z\text{-angle}}$, and intertube vdW interactions, $\sigma_{z\text{-vdW}}$.

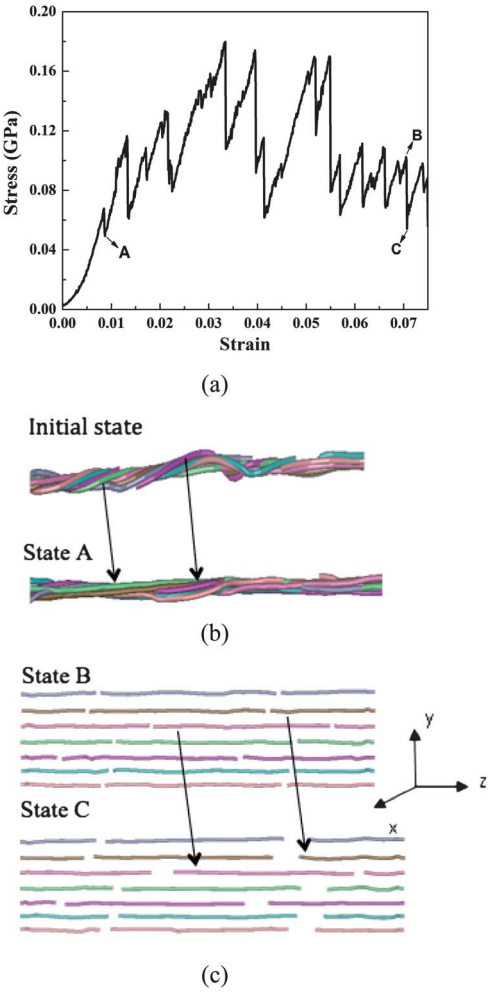

Fig. 8 (a) Stress–strain curve of a random CNT fiber under tension. (b) Illustration of the fiber untwisting from the initial state to state A (the fiber length is scaled down for improved visualization). (c) Intertube sliding from state B to state C (the CNTs are translated perpendicular to the *xz* plane for better illustration).

strain of 0.0083 (state A), the tensile stress increases gradually with strain. While in the second stage starting from state A, the stress oscillates between maximum and minimum values.

The structural evolution mechanism of the twisted fiber under tension can be divided into three categories: CNT stretching, fiber untwisting and intertube sliding. Since the CNTs are bent and contact partially with each other through vdW interactions after twisting, CNTs in the fiber initially undergo stretching and untwisting under fiber tension, as shown in Fig. 8b, which results in the gradual increase of fiber stress. Under higher tensile stress (*i.e.* in the second stage), the intertube sliding takes place because the vdW interactions are inadequate to maintain the present fiber structure, as illustrated in Fig. 8c. The intertube sliding is the main reason for the sudden drop of stress in the second stage.

The structural evolution mechanism of fibers with regular CNT stacking is similar to that of fibers with random CNT stacking, wherein CNT stretching, fiber untwisting and intertube sliding are the main deformation modes. However, the difference in their tensile response is also obvious as explained below. The load-carrying capability in the overlapped areas is governed by the weak vdWs interactions, while in the non-overlapped areas it is governed by the strong bonding interactions of interbeads. The overlapped areas form the weak points in the films and fibers. The main distinction between fibers with regular CNT stacking and random CNT stacking is that the weak points are concentrated in the former case, while randomly distributed in the latter case. Consequently, the regular stacking CNT fiber breaks at the weakest section in a brittle manner, while the random stacking CNT fiber breaks ductilely, as shown in Fig. 9a and b, respectively.

3.5 Strength enhancement

Based on the aforementioned simulation results, it can be concluded that enhancing intertube interactions could postpone the initiation of intertube sliding and allow for better redistribution of local stresses and strains among the CNTs, therefore leading to strengthening of the CNT fibers. Experimental results have also demonstrated that the intertube load transfer can be enhanced by surface functionalization[7,29] or irradiation-induced crosslinking.[30,31] According to eqn (3), intertube interactions can be strengthened by increasing the energy well depth at equilibrium ε. In the current study, ε is increased up to 6 times of the original value to evaluate its effect on the CNT fiber strength. The stress–strain relationships of the CNT fibers after such strengthening are plotted in Fig. 10. It is clearly shown that the strength of CNT fibers can be effectively improved without decreasing their failure strain through the enhancement of intertube interactions.

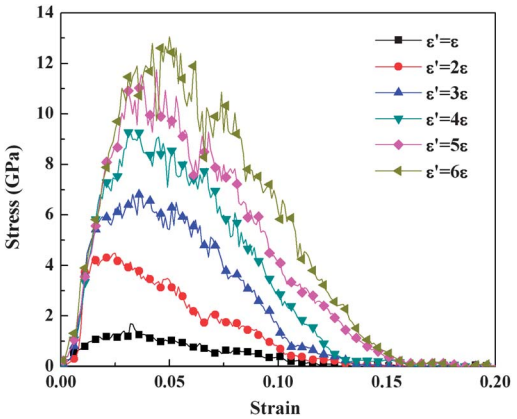

Fig. 10 Stress–strain relationships of CNT fibers (regular CNT stacking) with different intertube interactions.

4 Conclusion

Although enormous efforts have been devoted to the experimental characterization of the properties of CNT fibers, there is still a lack of comprehensive understanding of their formation mechanisms and interior structural evolution under loading. In this paper, it is the first time that a numerical simulation method has been used to illustrate the deformation mechanisms of CNT fibers and investigate their tensile behavior. It has been concluded that the tensile strength of CNT fibers with random CNT stacking is higher than that of CNT fibers with regular CNT stacking. Three microstructural evolution mechanisms, namely CNT stretching, fiber untwisting (or unbending of the CNTs) and intertube sliding, have been identified for describing the CNT fiber deformation. The twisting effect on the fiber strength has also been studied, and it is found that small twisting would enhance the fiber strength, while over twisting would have the opposite effect. Besides, it is also found that the strength of CNT fibers can be effectively improved through the enhancement of intertube interactions. These simulation results are helpful in the optimal design of CNT fiber performance.

Finally, it should be mentioned that in the current study, CNTs in the fibers were assumed to be straight. However, in reality, some CNTs are curved or even entangled with one another. Thus, this study should be considered as qualitative investigation of the tensile behavior of CNT fibers. The effect of CNT waviness and entanglement should be studied in the future. Modeling of CNT films/fibers with longer CNTs would provide more realistic simulation and optimization of CNT fiber properties. Besides, one potential limitation of the present CGMD method is that the radial deformation of the individual CNTs during the fiber deformation cannot be taken into

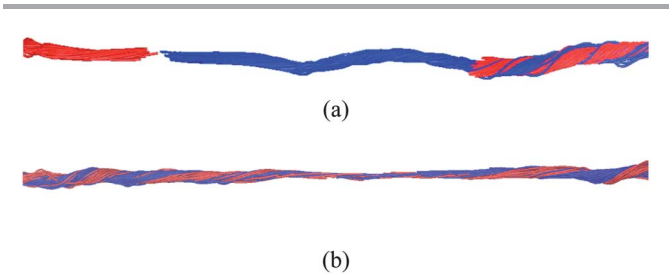

Fig. 9 Tension-induced failure of CNT fibers with (a) regular CNT stacking and (b) random CNT stacking.

account. Thus, this simulation method is not suitable for investigating the mechanical performance of CNT fibers with large diameter CNTs, wherein they are susceptible to radial deformation.

Acknowledgements

This work was partially supported by the US Air Force Office of Scientific Research (Dr Byung-Lip Lee, Program Director), the National Research Foundation of Korea (NRF) through a grant provided by the Korean Ministry of Education, Science and Technology (MEST) and the Office of Naval Research (Dr Yapa Rajapakse, Program Director). The authors thank Dr Amanda Wu for helpful discussions. Xia Liu's study abroad at the University of Delaware is supported by the State Scholarship Fund of the China Scholarship Council.

Notes and references

1 W. B. Lu, M. Zu, J. H. Byun, B. S. Kim and T. W. Chou, *Adv. Mater.*, 2012, **24**, 1805–1833.
2 K. Koziol, J. Vilatela, A. Moisala, M. Motta, P. Cunniff, M. Sennett and A. Windle, *Science*, 2007, **318**, 1892–1895.
3 K. L. Jiang, Q. Q. Li and S. S. Fan, *Nature*, 2002, **419**, 801.
4 X. B. Zhang, K. L. Jiang, C. Feng, P. Liu, L. N. Zhang, J. Kong, T. H. Zhang, Q. Q. Li and S. S. Fan, *Adv. Mater.*, 2006, **18**, 1505–1510.
5 F. Deng, W. B. Lu, H. Zhao, Y. T. Zhu, B. S. Kim and T. W. Chou, *Carbon*, 2011, **49**, 1752–1757.
6 M. Zu, Q. W. Li, Y. T. Zhu, M. Dey, G. J. Wang, W. B. Lu, J. M. Deitzel, J. W. Gillespie, J. H. Byun and T. W. Chou, *Carbon*, 2012, **50**, 1271–1279.
7 M. Zu, W. B. Lu, Q. W. Li, Y. T. Zhu, G. J. Wang and T. W. Chou, *ACS Nano*, 2012, **6**, 4288–4297.
8 M. Zhang, K. R. Atkinson and R. H. Baughman, *Science*, 2004, **306**, 1358–1361.
9 Q. W. Li, X. F. Zhang, R. F. DePaula, L. X. Zheng, Y. H. Zhao, L. Stan, T. G. Holesinger, P. N. Arendt, D. E. Peterson and Y. T. Zhu, *Adv. Mater.*, 2006, **18**, 3160–3163.
10 X. F. Zhang, Q. W. Li, Y. Tu, Y. Li, J. Y. Coulter, L. X. Zheng, Y. H. Zhao, Q. X. Jia, D. E. Peterson and Y. T. Zhu, *Small*, 2007, **3**, 244–248.
11 X. F. Zhang, Q. W. Li, T. G. Holesinger, P. N. Arendt, J. Y. Huang, P. D. Kirven, T. G. Clapp, R. F. DePaula, X. Z. Liao, Y. H. Zhao, L. Zheng, D. E. Peterson and Y. T. Zhu, *Adv. Mater.*, 2007, **19**, 4198–4201.
12 C. D. Tran, W. Humphries, S. M. Smith, C. Huynh and S. Lucas, *Carbon*, 2009, **47**, 2662–2670.
13 M. Zhang, S. L. Fang, A. A. Zakhidov, S. B. Lee, A. E. Aliev, C. D. Williams, K. R. Atkinson and R. H. Baughman, *Science*, 2005, **309**, 1215–1219.
14 K. Liu, Y. H. Sun, P. Liu, J. P. Wang, Q. Q. Li, S. S. Fan and K. L. Jiang, *Nanotechnology*, 2009, **20**, 335705.
15 C. P. Huynh and S. C. Hawkins, Understanding the synthesis of directly spinnable carbon nanotube forests, *Carbon*, 2010, **48**, 1105–1115.
16 K. Liu, Y. H. Sun, R. F. Zhou, H. Y. Zhu, J. P. Wang, L. Liu, S. S. Fan and K. L. Jiang, *Nanotechnology*, 2010, **21**, 045708.
17 M. H. Miao, J. McDonnell, L. Vuckovic and S. C. Hawkins, *Carbon*, 2010, **48**, 2802–2811.
18 S. L. Fang, M. Zhang, A. A. Zakhidov and R. H. Baughman, *J. Phys.: Condens. Matter*, 2010, **22**, 334221.
19 L. X. Zheng, G. Z. Sun and Z. Y. Zhan, *Small*, 2010, **6**, 132–137.
20 M. J. Buehler, *J. Mater. Res.*, 2006, **21**, 2855–2869.
21 S. Cranford and M. J. Buehler, *Int. J. Mater. Struct. Integr.*, 2009, **3**, 161–178.
22 B. Xie, Y. L. Liu, Y. T. Ding, Q. S. Zheng and Z. P. Xu, *Soft Matter*, 2011, **7**, 10039–10047.
23 X. D. Yang, P. F. He and H. J. Gao, *Nano Res.*, 2011, **4**, 1191–1198.
24 Y. Li and M. Kröger, *Carbon*, 2012, **50**, 1793–1806.
25 W. C. Steven and J. B. Markus, *Nanotechnology*, 2010, **21**, 265706.
26 A. N. Volkov and L. V. Zhigilei, Structural stability of carbon nanotube films: the role of bending buckling, *ACS Nano*, 2010, **4**, 6187–6195.
27 N. M. Albuquerque, *LAMMPS Molecular Dynamics Simulator*, S. N. Laboratories, http://lammps.sandia.gov/, 2011.
28 M. F. Yu, O. Lourie, M. J. Dyer, K. Moloni, T. F. Kelly and R. S. Ruoff, *Science*, 2000, **287**, 637–640.
29 C. Fang, J. N. Zhao, J. J. Jia, Z. G. Zhang, X. H. Zhang and Q. W. Li, *Appl. Phys. Lett.*, 2010, **97**, 181906.
30 A. Kis, A. Csanyi, J. P. Salvetat, T. N. Lee, E. Couteau, A. J. Kulik, W. Benoit, J. Brugger and L. Forro, *Nat. Mater.*, 2004, **3**, 153–157.
31 B. Peng, M. Locascio, P. Zapol, S. Y. Li, S. L. Mielke, G. C. Schatz and H. D. Espinosa, *Nat. Nanotechnol.*, 2008, **3**, 626–631.

